International Journal of Pharmacy and Biological Sciences
ISSN: 2321-3272 (Print), ISSN: 2230-7605 (Online)
IJPBS | Volume 8 | Issue 2 | APR-JUN | 2018 | 352-364
Research Article | Biological Sciences | Open Access | MCI Approved| ज्ञान-विज्ञान विमुक्तये
|UGC Approved Journal |

IMPACT OF SNP MUTATIONS ON THE STRUCTURAL AND FUNCTIONAL BEHAVIOUR OF CD44 ASSOCIATED WITH ORAL CANCER

M. Krishnaveni[1] and Syed Hussain Basha[2]

[1]Assistant Professor, Department of Biochemistry, Periyar University, Salem – 636 011.
[2] Innovative Informatica Technologies, Hyderabad - 500 049, India.

***Corresponding Author Email: logasarvesh@gmail.com**

ABSTRACT

Oral cancer is a most prevalent cancer worldwide. Natural products are promising resource nowadays in research. Hence, Quinine was selected for the present study. CD44, a trans-membrane glycoprotein is a main hyaluronic acid(HA)binding receptor, expressed in cells, exhibits high affinity towards HA, increasing tumorigenesis. Altered CD44 glucosylation site, affects binding. Hence, computational modelling, simulation approach is applied to understand the effect of variants on the overall structure, functionality of the CD44.Present study demonstrates, T27A mutations affecting the protein structural stability hindering the function. Our simulation studies for CD44 in complex with quinine a natural compound, in its wild type and T27A mutant version state elucidated that due to mutation, protein has lost the required conformational space to recognize, bind the Quinine potentially tight,but not with wild state.

KEY WORDS

Oral cancer, Mutation, CD44 protein, MD simulations, Quinine.

INTRODUCTION

Oral Squamous Cell Carcinoma (OSCC) is most prevalent cancer worldwide with noticeable human death rate.The survival rate of the disease has not increased though the advancements in the treatment as surgery and chemo-radio therapy. The major cause of failure to cure this OSCC could be the resistance towards therapies reoccurrence [1]. Hyaluronan major component of extra cellular matrix and ligand for CD44 plays significant role in oral squamous cell carcinoma progression [2].CD44, a trans-membrane glycoprotein, hyaluronic binding receptor, expressed in a wide variety of cells [3, 4, 5]. Previously it was reported the use of CD44 as a marker for early molecular diagnosis of lung [6], prostate [7], colorectal [8], breast [9], gynaecologic [10], gastric [11], head and neck cancer [12], lymphoma [13], osteosarcoma [14]. Changes in CD44 Glucosylation site alters CD44 binding to hyaluronic acid, any mutations in the phosphorylation site of cytoplasmic domain of CD44 hinder its adhesion function. Chou reported chemoresistance in functional CD44 variants, compared to wild type carriers [15]. In this scenario, we have carried out this present modelling and simulations study to understand the mutational changes on the overall structure, functionality of CD44. Although, many mutations were reported for functional damage to the protein. we have selected six major mutations i.e, T27A, R41A, T102A,S112A,S122A,R162A reported around the glycosylation site of CD44 based on the importance on its functionality keeping in view of the complete crystallized structure accessibility [16].

MATERIALS AND METHODS

Selection of Single Nucleotide Polymorphism (SNPs) for in silico analysis

Human CD44 gene information data was collected from Online Mendelian Inheritance in Man [17] and Entrez Gene on National Centre for Biological Information (NCBI) dbSNP was used to take SNPs reported in CD44 gene associated with Oral cancer [18].6 SNPs were analysed further.The CD44 proteins amino acid sequence was retrieved from the Uniprot database(P16070).Protein 3D structure from protein data bank (1UUH) [19].

Mutant protein modeling

For a protein 3D structure is central to analyze its functionality, effect of SNP's. rcsb.org identifies the protein coded by CD44 gene (PDB ID 1UUH), comprising 158 amino acids. Six mutations were studied using "mutate a residue" in the Schrödinger maestro v9.6 visualization program.

MD simulations in water

Simulations were run in "Desmondv3.6 Package" [20, 21]. Water molecule simulated by predefined TIP3P [22]. Orthorhombic interval periphery state was set up for shape, size indication, replicating unit shield at a distance of 10Å.System was neutralized electrically, with suitable counter Na+/Cl- ion addition to balance charge, kept at random in solvated system. After this, minimization, relaxation of protein/protein-ligand complex under NPT ensemble via default practice of Desmond [23, 24] which includes 9 stages, only 2 minimization and 4 short simulations (equilibration phase) are involved before starting the actual production time.

Summary of simulation stages

Simulation was initiated by setting up periodic boundary conditions in NPT unit through OPLS 2005 force field element [28,29]. The temperature maintained was 300K and 1 atmospheric pressure via Nose-Hoover temperature coupling, isotropic scaling [25]. This was followed by running 10ns NPT production simulation each and saving the arrangements obtained at 5ps gap.

Analysis of molecular dynamics (MD) trajectory

These were analysed by using simulation quality, event, simulation interaction diagram programs of Desmond for calculating Energies, root-mean-square deviation, fluctuation. Total intramolecular hydrogen bonds, radius of gyration, secondary structure elements of protein conferring stability. These validates the system stability throughout the simulated length of chemical time for the given temperature, pressure, volume of the total simulation box as well as each frame of simulated trajectory output and the total secondary structure elements change in the protein structure during simulation.

Pre-processing and preparation

protein target structure

Crystal structure of CD44 protein in complex with hyaluronic acid was resolved by X-ray diffraction, with a resolution factor of 2.30Å was retrieved from Protein Data Bank [26] which was further modified for docking calculations as follows:CD44 protein was imported to Maestrov9.6.Making use of Protein preparation wizard, Schrödinger [27] included biological units and assigned bond orders, created zero-order bonds to metals, disulfide bonds, added missing hydrogens and capped termini, converted to methionines from its selenoform, deleted all water molecules, generated metal binding states for hetero atoms. Also verified for missing side chains, loops to fill via prime module integrated inside parallel plate waveguide (PPW) simulator and none was observed. Using refine tab all co-crystallized ligands and waters were identified and removed from the structure, the optimization of H-bond network to fix overlapping hydrogens, protonation states, hydroxyl hydrogen atoms, most likely positions of thiol, tautomers of 'His' residues, Chi 'flip' assignments for 'Gln', 'Asn','His' residue selection was done by protein assignment script of Schrodinger. At pH7.0, the protein was minimized by applying OPLS2005 force field [28, 29]. Controlled minimization was done until the average root mean square deviation of the non-hydrogen atoms are 0.30Å.

Ligand and docking

The 3D coordinates of quinine were retrieved from Pubchem database. Ligands for docking studies were prepared using Autodock mgltoolsv1.4.6. Before ligand preparation, ligand structure was energy minimized by charmm's force field. Ionization state was set to generate all possible states at pH7.0 ± 2.0. Keeping in view, the flexibility of rings per ligand, its chance to alter conformations all through docking calculations, we have specified to generate low energy ring conformation via allowing maximum possible rotatable bonds. Autodock Version 4.0 is used to predict binding pose with associated energy of the quinine compound with CD44 wild type protein as well as targeting the most damaging mutation found out through the simulation studies to know the effect of mutations on the binding of this natural inhibitor. Protocol followed for carrying out the docking studies using Autodock version 4.0 in

order to predict binding pose and IC50 values along with associated binding energies is of default parameters**.** Briefly, the energy scoring grid box was set to 126, 126 and 126 Å (x, y, and z) centered at X = -1.4938; Y = -4.1771 and Z = -1.0507 with 0.375 angstroms grid points spacing assigned with default atomic salvation parameters. The grid box was designed such that the total CD44 protein domain was surrounded by the three-dimensional grid box cantered at its own. Lamarckian Genetic Algorithm (LGA) forms a docking engine, with all parameters set to default. After each LGA run, Auto dock reports the best docking pose along with associated binding energy values for each docked complex, and the results are reported based on cluster analysis. Binding Gibbs free energy (ΔG) is calculated as a sum of six energy terms of dispersion/repulsion, electrostatic interactions, hydrogen bonding, deviation from covalent geometry, desolvation effects and internal ligand torsional constraints. From a total of 10 docking modes represented by LGA cluster analysis, the lowest energy docking mode with respective IC50 prediction was selected from each docking simulation. Each compound was allowed with active rotatable bonds making them flexible.

RESULTS AND DISCUSSION

Effect of SNPs on polarity, hydrophobicity, structural stability and functionality of the protein

Each amino acid has its own unique properties, such as molecular weight, size, polarity/charge and hydrophobicity values. In view of this fact, we have studied the effect of SNPs on the protein structure, but paid more attention to its polarity and hydrophobicity, since they are the major contributors for the protein's structure and functionality. The results of the detailed analysis for effect of mutations on protein's polarity and hydrophobicity are presented in Table.1.

Table 1: Mutations in CD44 associated oral cancer – Effect of the mutations on the change in polarity and hydrophobicity

S.No	Protein	Polarity	Change in polarity due to mutation	Hydrophobicity	Change in Hydrophobicity due to mutation
1.	T27A	Polar to non-polar	Yes	Hydrophilic to Hydrophobic	Yes
2.	R41A	Polar to non-polar	Yes	Hydrophilic to Hydrophobic	Yes
3.	T102A	Polar to non-polar	Yes	Hydrophilic to Hydrophobic	Yes
4.	S112A	Polar to non-polar	Yes	Hydrophilic to Hydrophobic	Yes
5.	S122A	Polar to non-polar	Yes	Hydrophilic to Hydrophobic	Yes
6.	R162A	Polar to non-polar	Yes	Hydrophilic to Hydrophobic	Yes

From the analysis it was revealed that, all the six mutations have shown polarity changes. On the other hand, potentially hydrogen bond forming residues, serine and threonine, were found to be mutated with non-hydrogen bond forming amino acid alanine, and is thus rarely directly involved in protein function, but it can play a role in substrate recognition or specificity. Arginine also mutated as alanine at 41 and 162 positions, these two residues critical for the interaction with substrate binding as they are more in protein active or binding sites. Arginine contains a complex guanidinium group on its side chain that has a geometry and charge distribution that is ideal for binding negatively-charged groups (it is able to form multiple hydrogen bonds) to create stabilizing hydrogen bonds that can be important for protein stability.

The above predictions were based on the standard evaluations that Glutamine (Q); Asparagine (N); Histidine (H); Serine (S); Threonine (T); Tyrosine (Y); Cysteine (C); Methionine (M); Tryptophan (W) were all potentially hydrogen bond-forming residues. Polarity changes in the protein, due to the above-mentioned mutations, might cause severe malfunctions in the protein with even minor changes in pH conditions.

Moreover, the six mutations that were mentioned above were found to be altered from hydrophobic residues to hydrophilic ones.

3.3 MD simulations

In order to understand the impact of these mutations on the overall protein conformational stability comparatively, we have carried out 10 nanoseconds of MDs for each protein. Various parameters have been analysed throughout the simulation trajectory, especially Root mean square deviation (RMSD), Root mean square fluctuations (RMSF), energy parameters, total number of intra -molecular hydrogen bonds, radius of gyration and the secondary structure elements (SSE) of the protein with the time dependent function of MDs for our quantity analysis. Chemical time scale used in this present study is of enough for the side chain rearrangements in protein's backbone to facilitate various conformations. The detailed MD simulations were depicted in Table.2.

Table 2: MD simulation statistics

Protein	Graph color code	Energy		RMSD		ROG		Intra H-Bonds	
		Range	Mean	Range	Mean	Range	Mean	Range	Mean
CD44 apo	Blue	[-4551.315, -3655.784]	-4166.838	[0.000, 2.382]	1.345	[14.780, 15.493]	15.036	[96.000, 133.000]	113.310
T27A	Red	[-4811.153, -3971.391]	-4358.253	[0.000, 2.606]	1.814	[14.853, 15.716]	15.368	[94.000, 126.000]	111.845
R41A	Green	[-4748.709, -3771.636]	-4279.806	[0.000, 2.662]	1.659	[14.773, 15.942]	15.326	[90.000, 132.000]	106.194
T102A	Yellow	[-4549.427, -3897.624]	-4231.241	[0.000, 2.226]	1.472	[14.845, 15.334]	15.081	[95.000, 130.000]	110.966
S112A	Pink	[-4549.688, -3698.265]	-4157.115	[0.000, 1.625]	1.191	[14.750, 15.251]	14.993	[98.000, 132.000]	113.172
S122A	Black	[-4665.187, -3704.173]	-4226.500	[0.000, 2.331]	1.377	[14.854, 15.410]	15.096	[98.000, 129.000]	112.856
R162A	Brown	[-4487.203, -3954.838]	-4238.485	[0.000, 1.982]	1.426	[14.889, 15.371]	15.094	[100.000, 126.000]	113.737

3.4 Protein structure conformational flexibility and stability analysis

RMSD values of wild type, mutant proteins were analysed, to understand the effect of mutations on the protein structure. We calculated the RMSD for all protein backbones during the MDS with reference to its initial structure (Fig.1). However, the wild type protein was found to be stabilized at an RMSD value of 1.345 Å, whereas most of the mutant protein RMSD values were higher than the wild type, with exception of S112A which were lower than the wild type protein's RMSD at certain points.

In Figure 1, T27A and R162A mutated structures showing maximum deviation till the end of the simulation compare to wild-type. These two mutants remained distinguished throughout the simulation resulting in maximum backbone RMSD of ~2.6 Å. This difference in the deviation range explains the change in stability of the mutant protein, which in turn reflects the impact of substituted amino acid in the protein structure. T102A and R41A mutated structures showing minimum deviation compared to wild type, but R41A showing highest deviation from 6000 ps to till the end, resulting in a backbone RMSD of ~ 1.0 to 2.662 Å during the simulations. S112A and S122A mutated structures were not showing much deviation compared to wild type, but S122A showing mild deviation at 3000 ps. Figure. 3 clearly demonstrate that the mutations have considerable destabilizing effects on protein structure. RMSD in the mutant is higher than the wild type, indicating that excessive flexibility is gained after the mutation.

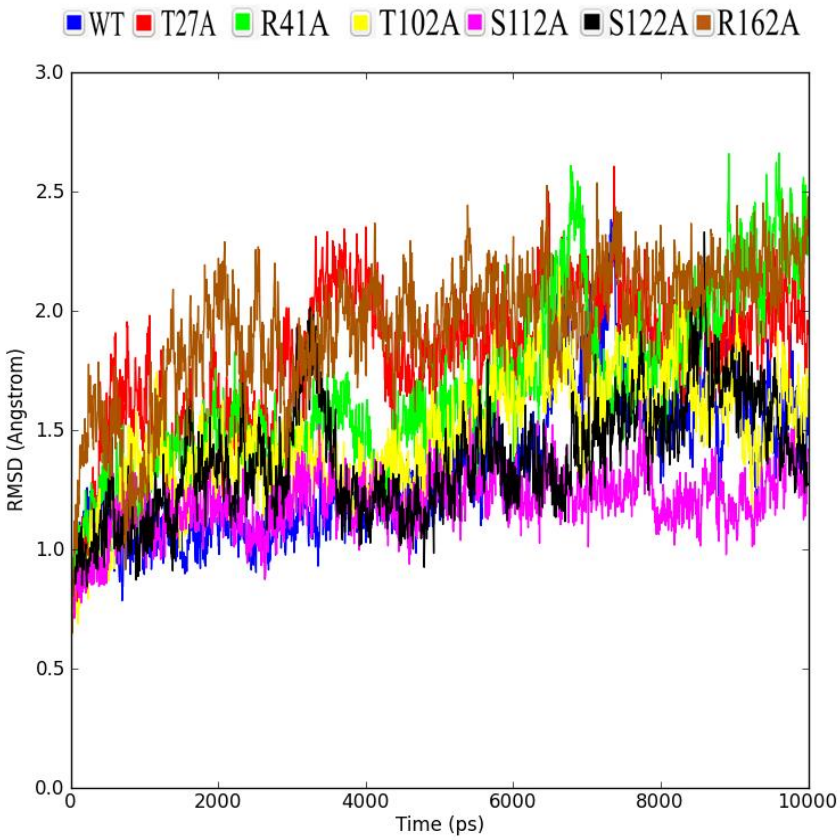

Figure 1: RMSD graphs of the CD44 wild type protein compared with the mutant versions of the protein.

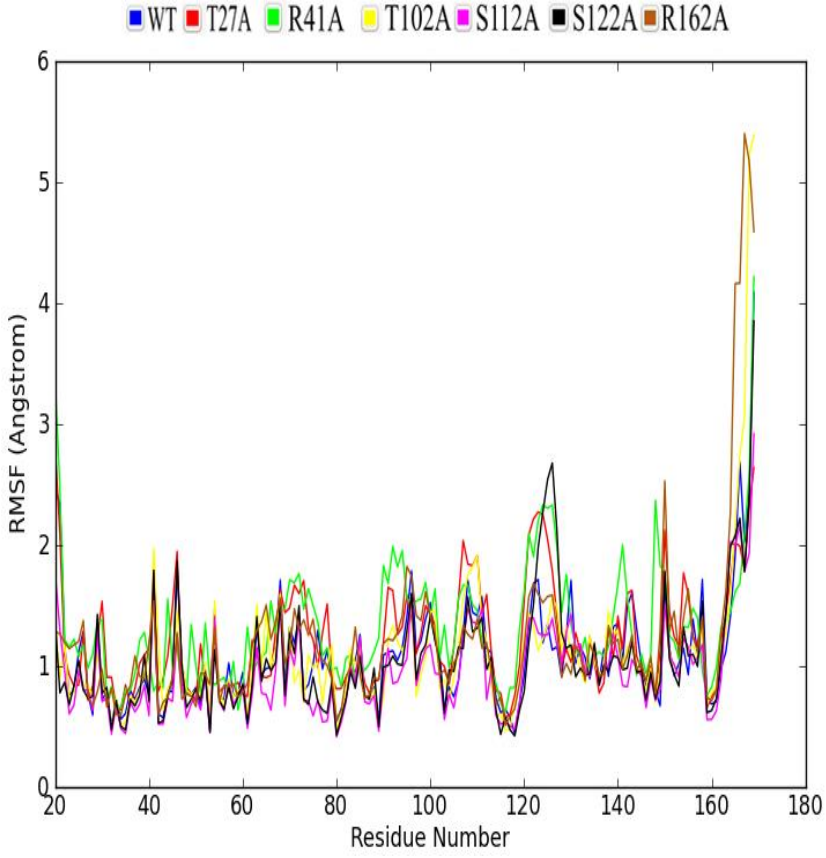

Figure 2: RMSF graphs of the CD44 wild type protein compared with the mutant versions of the protein

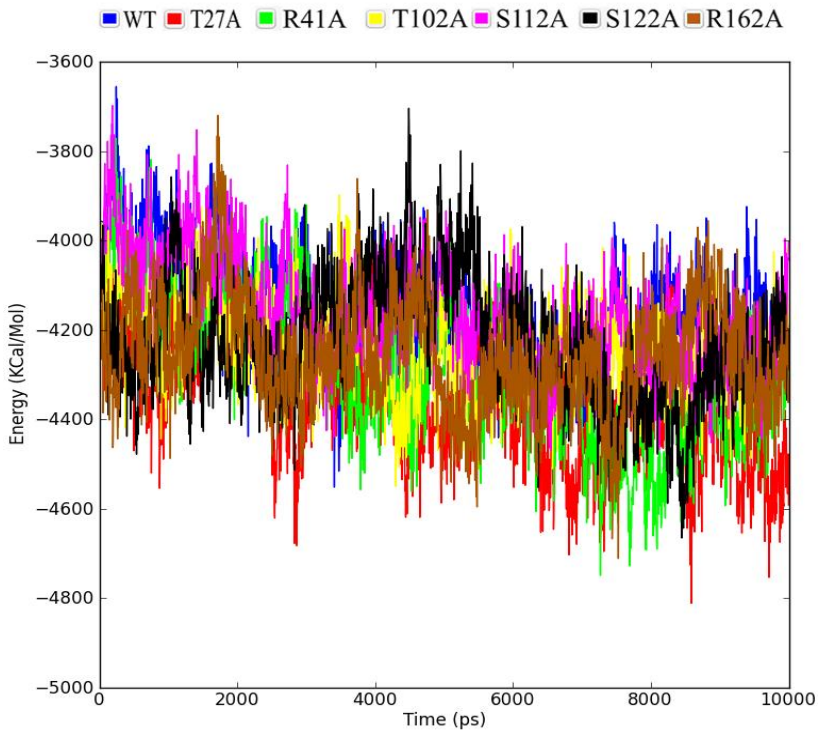

Figure 3: Energy graphs of the CD44 wild type protein compared with the mutant versions of the protein.

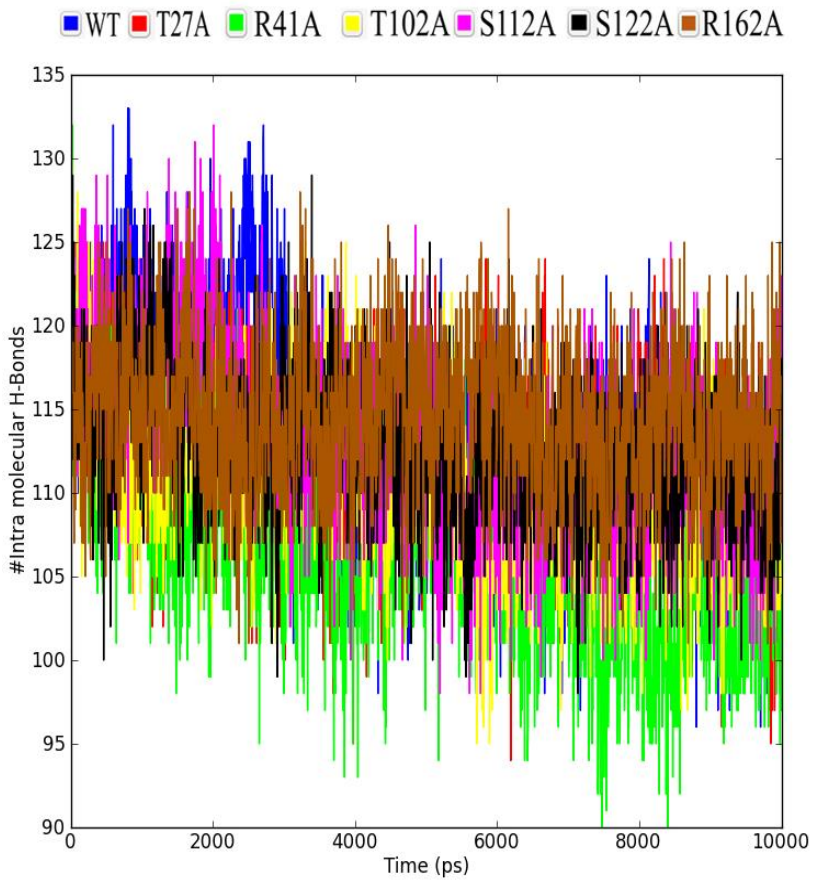

Figure 4: Total number of intra molecular hydrogen bonds graphs of the CD44 wild type protein compared with the mutant versions of the protein.

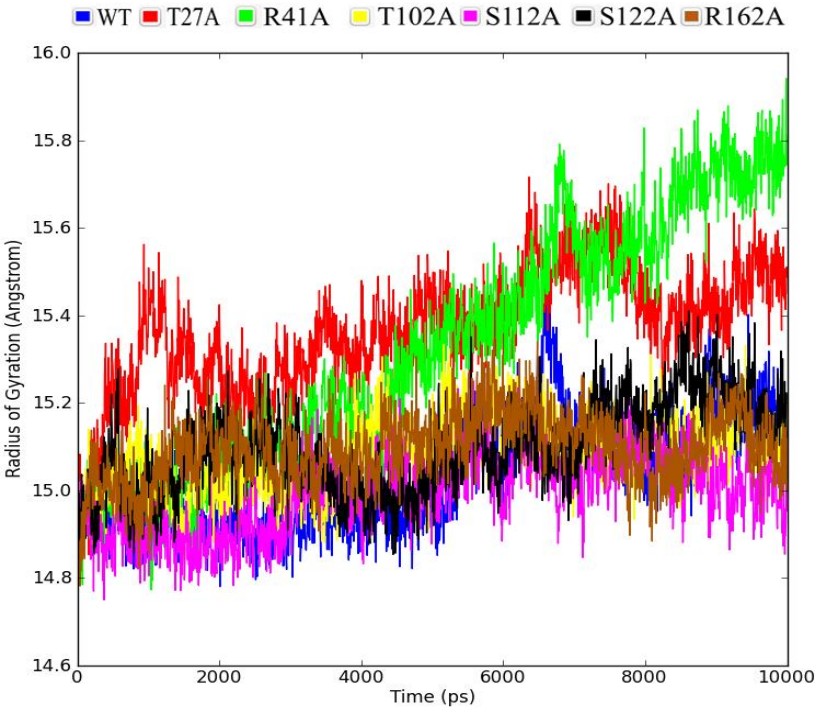

Figure 5: Radius of Gyration graphs of the CD44 wild type protein compared with the mutant versions of the protein.

We have also monitored the RMSF fluctuations of each residue in order to determine the mutation's effect on the protein residues dynamic behaviour of residues. From Figure.2 it can be inferred that residue level fluctuations for T27A, R41A, and S122A were quite high when compared with wild-type and other mutations up to 2.8 Å, for residues located between 120 and 150 positions. Analysis of the fluctuations revealed that the greatest degree of flexibility was shown by the T27A mutant protein.

When the energy parameters for the MD simulation trajectories of the wild type along with associated mutated proteins were analysed and revealed that they were maintaining the total energy of the system in a range of -4358 and -4157 Kcal/mol (Fig. 3). Whereas, for the wild type protein the energy system was -4166 Kcal/mol of. Among the above-mentioned energies, S112A mutated protein was showing the least possible minimized total energy of -4157 Kcal/mol, whereas the highest energy of -4358 Kcal/mol was consumed by T27A mutation. From the results, it is clear that as the mutation residue position increases, the total energy of the system increases as well, suggesting that the mutations occurring at the core of the protein structure would further minimize its overall energy.

We also analysed the intra-molecular hydrogen bonds in the protein along with its reported mutations contributing for their stability (Fig. 4). From Table 2 it can be inferred that the maximum number of 113 intra-molecular hydrogen bonds was observed for wild type, S112, and R162A proteins and the T27A, R41A, T102A, and S122A Proteins have 111, 106, 110 and 112 intra-molecular hydrogen bonds respectively. The least number of 106 intra H-bonds were found for R41A mutation. This data suggests that T27A, R41A and T102A mutations have higher flexibility compared to other mutations and wild type protein.

The radius of gyration (Rg) is the mass-weight root-mean-square distance of collection of atoms from their common centre of mass. Therefore, it provides an insight into the overall dimension of the protein. Finally, we have analysed the radius of gyration (ROG) for the wild-type protein along with its associated mutations contributing to their compactness (Fig. 5). From graphs it can be inferred that six mutant proteins not showing much difference compared to wild type when considering the statistical data, however T27A mutation has shown the highest compactness in the protein with 15.368 Å, whereas the wild type protein has shown to be compacted with 15.068 Å. These data suggest that T27A mutation has caused structural destabilizing effects leading to the loss of protein compactness when compared to the data with wild type ROG.

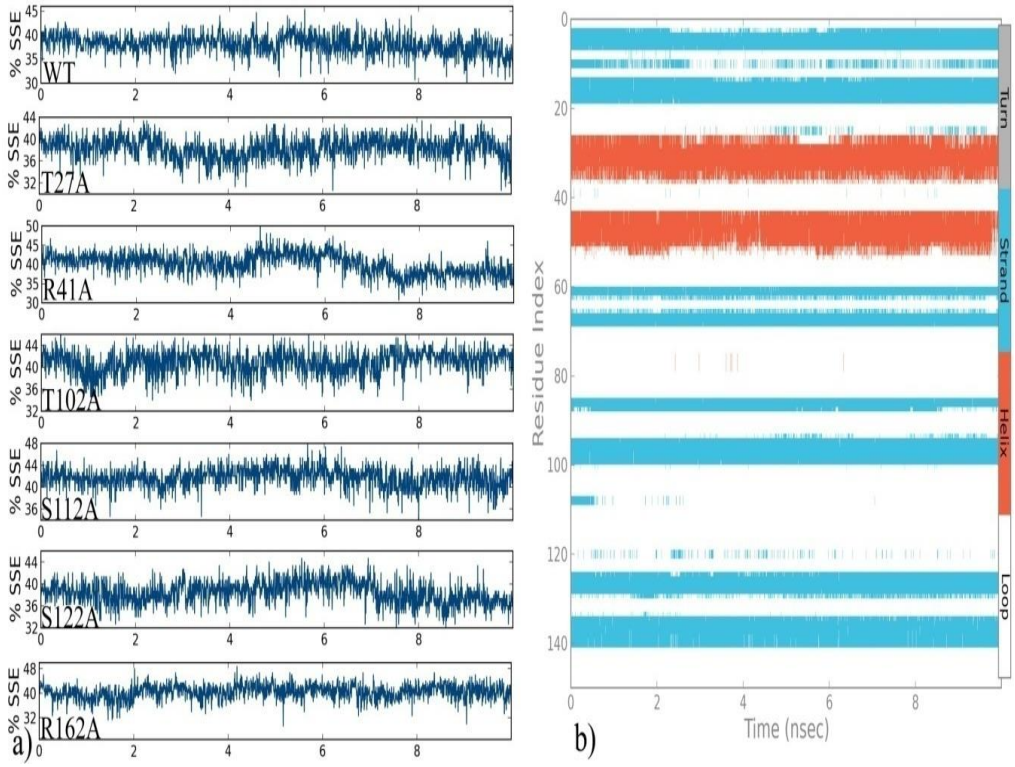

Figure 6: a) Secondary structure elements (SSE) graphs of the CD44 wild type protein compared with the mutant versions of the protein. b) Detailed Secondary structure elements (SSE) graph of T27A mutant version of CD44.

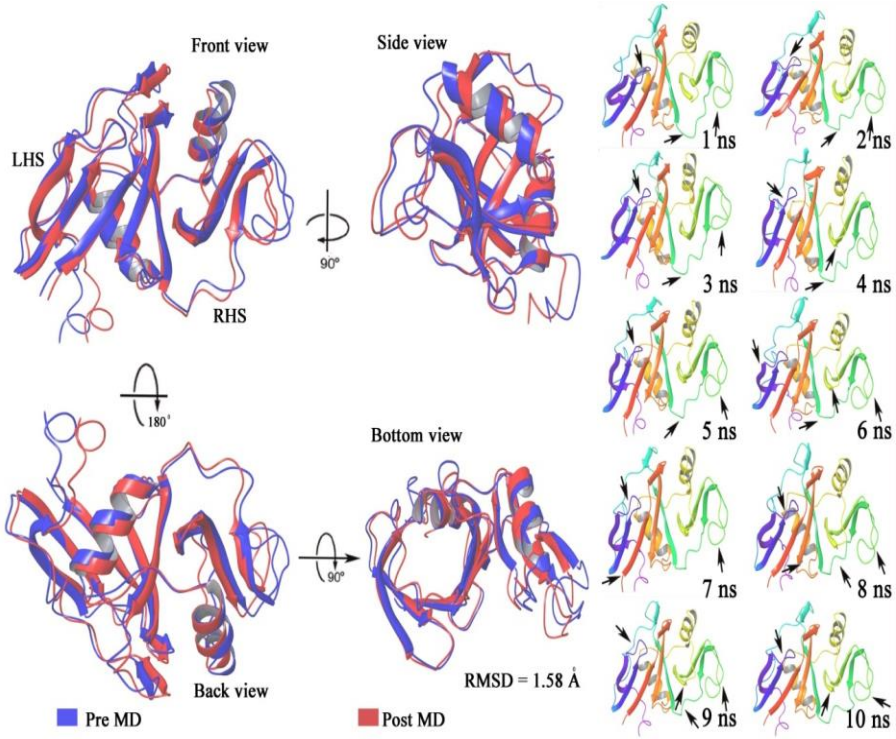

Figure 7: Superimposition of pre and post MD simulation snapshots of CD44 in its T27A mutant state pointing some of the structural features movement observed which were thought to be crucial in CD44 overall structural stability.

When the secondary structure elements (SSE) contributing to the overall protein stability were analysed, it was observed that all the proteins were maintaining an average of around 64% SSE, mostly composed of helices rather than strands and loops, with an exception of R161P mutation. When we further investigated R161P was showing 60% SSE it is less when compare (Fig.6) with the wild type and other mutants. There are no noticeable changes in their residual level as the general profile of residual fluctuation of wild-type and mutants are minimal in each protein without any abnormal fluctuation. From these MD simulation-based analysis it was revealed that T27A mutation has higher impact on the CD44 protein structure stability causing hindrance in its functionality due to the changes in its overall structural features (Figure 7). Higher flexibility and major structural changes observed in T27A mutant version of protein suggests decrease in stability of the protein which is a direct indication towards its possible loss or decreased functionality.

CD44-Quinine docking analysis

Recently, a considerable amount of literature has suggested high potent activity of quinine compound against cancer. In continuation to the quest of understanding the potential of this natural compound, we have recently performed a lab scale study to evaluate the anticancer effects of quinine on KB and HEp-2 cancer cells. Our MTT assay-based studies has revealed that quinine has an IC50 value of 125.23µm for 24hr and 117.81µm for 48hr with respect to KB cell line. Whereas, it was 147.58µm and 123.74µm with Hep2 [30]. Quinine was reported for reduced iNOS, COX-2, IL-6, Bcl-2, mutant p53 and up-regulated Bax, caspase-3 expressions suggesting its antiproliferative role [31]. In this scenario, taking our present study to a step further, we have investigated the impact of mutations on the inhibitor recognition functions of CD44 protein, docking analysis was carried out with specific inhibitor quinine indicated that the mutations contribute to weaker interaction with the drug, primarily due to loss of interactions of the drug with surrounding residues. We utilised wild-type (CD44-quinine), T27A(T27A-quinine) for our analysis (Figure.8).

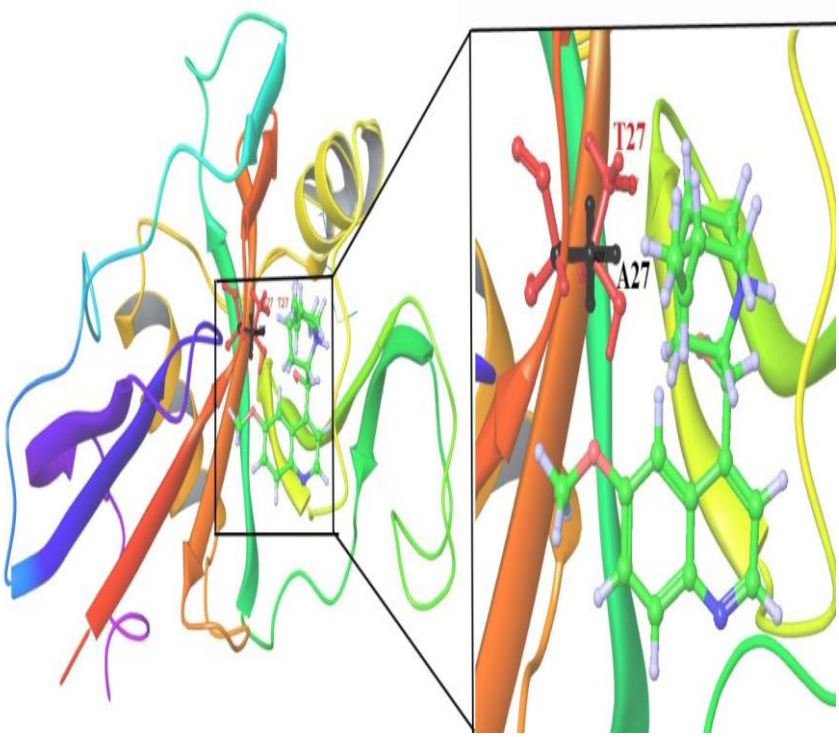

Figure 8: Docking pose of quinine compound inside the active binding site of CD44 showing the mutant residue T27A.

Comparing the binding free energy of CD44 to the drug, mutant T27A exhibited the weakest interaction with the energy value of −5.58 Kcal/mol with 81.25µm of inhibition constant when compared to wild-type complex -6.05 Kcal/mol with 36. 62µm.This result signifies better conjugation of inhibitor to the binding pocket of the receptor. Mutant T27A complex exhibited

the least binding affinity towards quinine according to the docking score results.

Protein-ligand MD simulations in water

Since molecular docking represents only a single snapshot of protein–ligand interactions, we have performed molecular dynamic simulations in order to study the protein–ligand interactions in motion contributing for their stable bound conformation and to visualize the effect of ligand binding on protein conformational changes. The effect of quinine on wild-type CD44 and T27A mutant was studied through MD simulations.

Simulation studies using Quinine with wild and T27A mutant

The dynamic behaviour of wild and mutant protein via simulations. The RMSD contributions were plotted as the time dependant function of MD simulations between the wild-type and mutant (T27A). Two independent simulations were carried out.

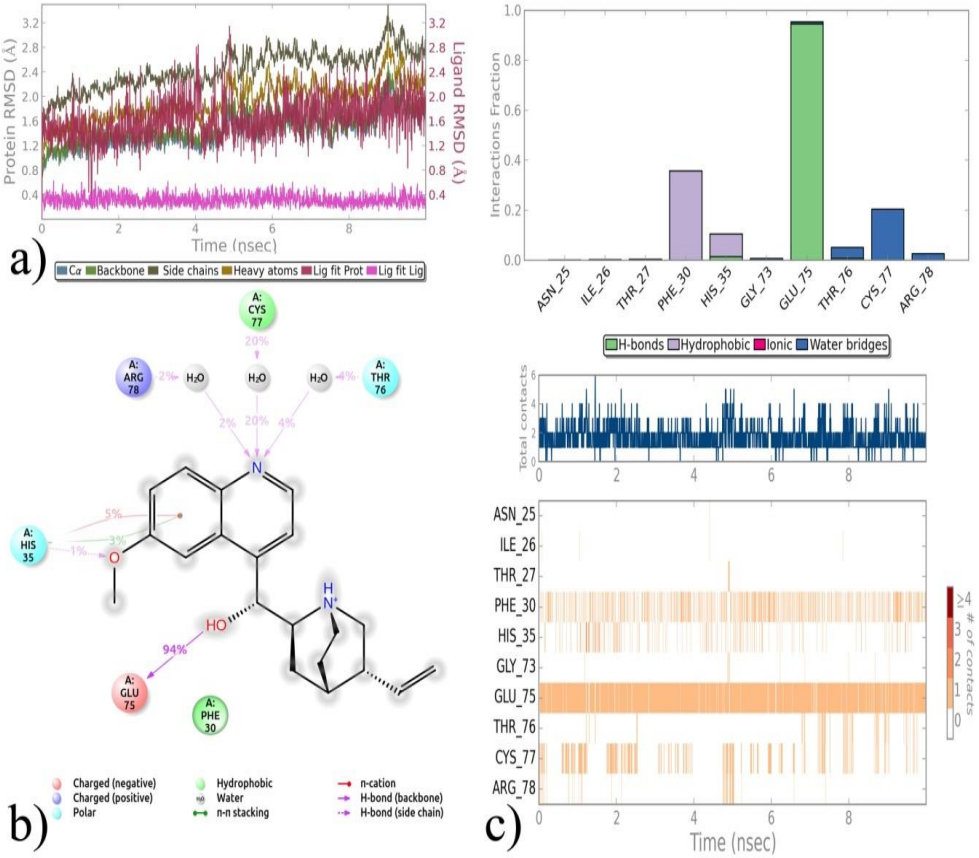

Figure 9: MD simulation revealed interactions of CD44 with quinine compound in its wild state (without any mutation).

The results in Figure 9 shows that the RMSDs of the trajectories for the wild-type complex was well below 3.0Å for the first 5ns.Throughout the simulation period, no significant fluctuations were observed in the backbone of the wild-type implying that the binding of quinine at the active site of the proteins is not only stable and strong but also does not disturb the protein backbone stability. When mutant protein residue fluctuations were calculated in presence of ligand quinine, it was observed that movements and continuous fluctuations noticeable at 1ns (Fig 9b). RMSD value of the ligand observed in the figure is significantly larger than the RMSD of the protein. According to this observation the ligand has diffused away from its initial binding site in the early simulations, which leads to the inefficient binding with T27A mutant protein. Indeed, wild-type and mutant complex reaches a steady equilibrium except T27A. Mutant T27A remain different throughout the simulation, resulting in greatest backbone RMSD of ~3.2Å. This deviation range difference make clear the alteration in the stability of mutant protein, which further reveal the strength of substituted amino acid in protein structure.

In order to calculate the residual mobility of each lead molecules in CD44 protein–ligand complexes (wild-type and mutant), RMSF was calculated in each complex and

the graph was plotted against the residue number based on the trajectory period of MD simulation to identify the higher flexibility regions in the protein. In protein RMSF graph of mutant complex, we can see that the major peaks of fluctuations have been observed with 120-125 residues with over 4Å, and residues between 140-145 with >4.2Å have highest deviation during the MD simulations. Rest of the residues were found to be quite stable and fluctuating well below 2.0Å.Despite the fact that mutant complex T27A showed deviation from its starting conformation. Analysis of fluctuation score depicted that the higher degree of flexibility was observed in mutant (T27A) complex than wild-type structure suggesting altered binding of quinine with T27A, thereby making the backbone more flexible to move. We also monitor changes in secondary structure during the simulations, it was observed that wild-type and mutant proteins maintaining an average of around 64%, there is no significant change observed in the secondary structure of mutant complex (Figure 10).

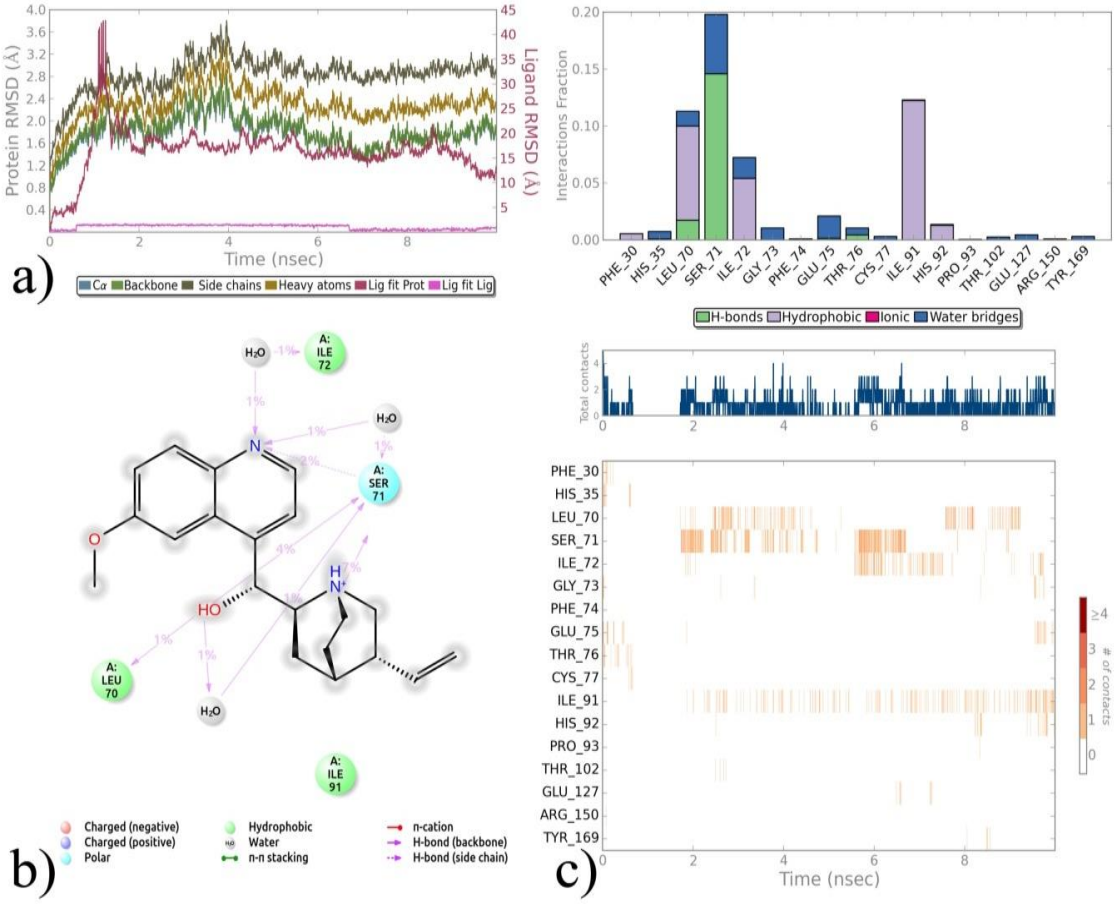

Figure 10: MD simulation revealed interactions of CD44 with quinine compound in its T27A mutation state.

From our analysis, it is well revealed that wild-type complex form strong hydrogen bond with quinine and it is maintained throughout the simulation, while the mutant complex T27A showing very weak intermolecular hydrogen bonds and these bonds were not maintained thorough out the simulation time. Hydrogen bonds in the wild-type complex helps in maintaining its rigidity, which was not so with mutant. T27A mutation showed increased binding energy, loss of hydrogen bond interactions i.e stability loss when compared with wild-type CD44 protein.

Interaction profile of ligand with wild and mutant during MD simulation

When one of the best snapshots of MD trajectory was analysed, it has been observed that quinine forming strong hydrogen bond with GLU 75 residue at catalytic site of wild-type CD44 protein with over 94% occupancy, but mutant protein was not forming hydrogen bonds with GLU 75 residue whereas it was trying to form hydrogen bond with SER71 with over 2% occupancy only during MD trajectory (Figure 9). Results of the hydrophobic interactions of the ligand with wild-type protein shows, that it was found to be interacting with Phe30, His 35 and in the mutant protein MD simulations

forms hydrophobic interactions with Leu70, Ile91 but these interactions not maintaining at least 10% of the MD simulation time. From the total contacts formed between quinine with wild-type and T27A mutant CD44 residues, wild-type was found to be in contact with residues Asn25, Ile26, Thr27, Phe30, His35, Gly73, Glu75, Thr76, Cys77, Arg78 and mutant protein was found to be in contact with residues Phe30, His35, Leu70, Ser71, Ile72, Gly73, Phe74, Glu75, Thr76, Cys77, Ile91, His92, Pro93, Thr102, Glu127, Arg150, Tyr169 (Figure10). Quinine trying to contact more amino acids of mutant complex compared to wild-type during MD simulation. T27A mutant complex residues were not able to form strong contact with quinine due to this less interactions in T27 mutant structure. Further, from our study it is clear that the mutant model T27A has higher overall flexibility when compared to the native protein. RMSF of ligand shows, how ligand fragment work together with the protein and their entropic nature. Mutant complex T27A showed a higher deviation with wild type. The number of hydrogen bonds formed between quinine and protein models (wild-type and mutant) during the MD simulation were also calculated.

CONCLUSION

The present study throws an insight into the six SNP connected with CD44 gene. MD trajectory revealed the probable malfunctioning mechanism via their structural destabilization. When wild type and all the selected mutations were compared, the T27A caused damage to the protein's structure. We studied the most damage mutant T27A CD44 and wild-type protein structures interactions with ligand quinine and explicit solvent behaviour of protein models in order to examine the difference in stability and dynamics behaviour. Moreover, the protein-ligand complex structures were validated by RMSD, RMSF, hydrogen bonds and salt bridge analysis. Results from the molecular dynamic simulations in water show that the trajectory of the T27A mutant protein complexed with ligand quinine was not stable over a time period of 10 ns, in comparison to the wild-type protein. Therefore, we would suggest that T27A mutation have impact on protein function. We expect that the results from the current computational approach on CD44 with suitable validation in near future will aid in having through knowledge on the effect of individual drug response and treatment of diseases especially in oral cancer. This study creates new direction for the design and development of even more potent inhibitors that are tailored too specific for CD44 mutants which might have been tried with Quinine by creating changes in functional groups.

Conflict of interest:

The authors declare that they have no conflict of interest.

Acknowledgement

REFERENCES

1. Mitra D., Malkoski SP., Wang XJ., Cancer stem cells in head and neck cancer. Cancers,3: 415-427, (2009).
2. Wang SJ., Earle C., Wong G., Bourguignon LY., Role of hyaluronan synthase 2 to promote CD44 dependent oral cavity squamous cell carcinoma progression. Head Neck, 35: 511-20, (2013).
3. Lesley J., Hyman R., Kincade PW., CD44 and its interaction with extracellular matrix.Adv. Immunol. 54: 271-335, (1993)
4. Lesley J., Hyman R., CD44 structure and function. Frontiers Biosci.3: 616-630, (1998).
5. Aruffo A, Stamenkovic I, Melnick M, Underhill CB, Seed B 1990 CD44 is the principal cell surface receptor for hyaluronate. Cell 61: 1303-1313.
6. Nguyen VN., Mirejovsk T., Melinova TL., Mandys V., CD44 and its v6 spliced variant in lung carcinomas: relation to NCAM, CEA, EMA and UP1 and prognostic significance. Neoplasma,. 47: 400- 408, (2000).
7. Desai B., Ma T., Zhu J., Chellaiah MA., Characterization of the expression of variant and standard CD44 in prostate cancer cells: identification of the possible molecular mechanism of CD44/MMP9 complex formation on the cell surface. J Cell Biochem, 108: 272-284, (2009) .
8. Kopp R., Fichter M., Assert R., Pfeiffer AF., Classen S., Butyrate-induced alterations of phosphoinositide metabolism, protein kinase C activity and reduced CD44 variant expression in HT-29 colon cancer cells. Int J Mol Med, 23: 639-649, (2009).
9. Auvinen R., Tammi M., Tammi R., Johansson V., Kosma M., Expression of CD44s, CD44v3 and CD44v6 in benign and malignant breast lesions: correlation and colocalization with hyaluronan. Histopathology, 47: 420-428, (2005).
10. Hong SC., Song JY., Lee JK., Lee NW., Kim SH., Yeom BW., Lee KW., Significance of CD44v6 expression in gynecologic malignancies. J Obstet Gynaecol Res, 32: 379-386, (2006).

11. Da Cunha CB., Oliveira C., Wen X., Gomes B., Sousa S., Suriano G., Grellier M., Huntsman DG., Carneiro F., Granja PL., Seruca R., De novo expression of CD44 variants in sporadic and hereditary gastric cancer. Lab. Invest, 90: 1604-1614, (2010).
12. Wang SJ., Wong G., de Heer AM., Xia W., Bourguignon LY., CD44 variant isoforms in head and neck squamous cell carcinoma progression. Laryngoscope 119: 1518-1530, (2009).
13. Nagel S., Hirschmann P., Dirnhofer S., Günthert U., Tzankov A., Coexpression of CD44 variant isoforms and receptor for hyaluronic acid-mediated motility [RHAMM, CD168] is an International Prognostic Index and C-MYC gene status-independent predictor of poor outcome in diffuse large B-cell lymphomas. Exp Hematol, 38:38-45, (2010).
14. Ma Q., Zhou Y., Ma B., Chen X., Wen Y., Liu Y., Fan Q., Qiu X., The clinical value of CXCR4, HER2 and CD44 in human osteosarcoma: A pilot study. Oncol Lett, 3:797–801, (2012).
15. Chou YE., Hsieh MJ., Hsin CH., Chiang WL., Lai YC., Lee YH., Huang SC., Yang SF., Lin CW., CD44 Gene Polymorphisms and Environmental Factors on Oral Cancer Susceptibility in Taiwan. PLoS ONE, 9: 93692, (2014).
16. Armando B., Nocks A., Aruffo A., Spring F., Stamenkovic I., "Glycosylation of CD44 is implicated in CD44 mediated cell adhesion to hyaluronan." The Journal of cell biology 132: 1199-1208, (1996).
17. Amberger J., Bocchini CA., Scott AF., Hamosh A., "McKusick's online mendelian inheritance in man." Nucleic Acids Res, 37: 1, 793-796, (1994).
18. Sherry ST., Ward MH., Kholodov M., Baker J., Phan L., Smigielski EM., Sirotkin K., DbSNP: the NCBI database of genetic variation. Nucleic Acids Res, 29: 308–311, (2001).
19. Peter T., Banerji S., Noble M., Charles DB., Alan JW., Andrew RP., David LE., Mahoney J., Tammi MI., Kahmann JD., Campbell ID., Day AJ., Jackson DG., Structure of the Regulatory Hyaluronan Binding Domain in the Inflammatory Leukocyte Homing Receptor CD44. Molecular Cell 13: 483-496, (2004).
20. Desmond Molecular Dynamics System, version 3.6, D E Shaw Research, New York, 2013.
21. Shivakumar D., Williams J., Wu Y., Damm W., Shelley J., Sherman W., Prediction of Absolute Solvation Free Energies using Molecular Dynamics Free Energy Perturbation and the OPLS Force Field. J Chem Theory Comput, 6: 1509, (2010).
22. Jorgensen WL.,Chandrasekhar J., Madura JD., Impey RW., Klein ML., Comparison of simple potential functions for simulating liquid water. JChemPhys,79:926-935, (1983).
23. Reddy SVG., Reddy KT., Kumari VV., Basha SH., Molecular docking and dynamic simulation studies evidenced plausible immunotherapeutic anticancer property by Withaferin A targeting indoleamine 2, 3-dioxygenase. J Biomol Struct, Dyn, 1-15, 2015.
24. Basha SH., Prakash B., Rambabu M., Firoz A., Viswanadha murty NVS., Sreenivasa reddy E., Anti-angiogenesis property by Quercetin compound targeting VEGFR2 elucidated in a computational approach. Euro J Biotech Biosci, 26: 30-46, (2014).
25. Shuichi N., A unified formulation of the constant temperature molecular dynamics methods. J Chem Phys, 81: 511, (1984).
26. Bernstein FC., Koetzle TF., Williams G J., Meyer EE., Jr. Brice MD., Rodgers JR., Tasumi M., The protein data bank: A computer-based archival file for macromolecular structures. J Mol Biol, 112: 535, (1977) .
27. Sastry GM., Adzhigirey M., Day T., Annabhimoju R., Sherman W., Protein and ligand preparation: parameters, protocols and influence on virtual screening enrichments. J Comput Aid Mol Des, 27:221-234, (2013).
28. Jorgensen WL., Maxwell DS., Tirado-Rives J., Development and testing of the OPLS all tom force field on conformational energetics and properties of organic liquids. J Am Chem Soc, 118:11225-11236, (1996).
29. Kaminski G., Friesner RA., Tirado-Rives J., Jorgensen WL., Evaluation and reparameterization of the OPLS-AA force field for proteins via comparison with accurate quantum chemical calculations on peptides. J Phys Chem, 105: 6474-6487, (2001).
30. Krishnaveni M., Suresh K., A Study on Protective Effect of Quinine against Lipid Peroxidation and Antioxidants Status in Human Oral Cancer Cell Line" Research Journal of Pharmaceutical, Biological and Chemical Sciences, 6: 295-301, (2015).
31. Krishnaveni M., Suresh K., Arunkumar R., Anti-proliferative and apoptotic effects of quinine in human Hep-2 laryngeal cancer and KB oral cancer cell." Bangladesh Journal of Pharmacology, 11:593-602, (2016).

***Corresponding Author:**
M. Krishnaveni*
Email: logasarvesh@gmail.com